Geometrical Variations of the Skeletal Structures of Genus *Pantanellium* as Determined from Collected Specimens

Takashi Yoshino[1] (tyoshino@toyo.jp, ORCID: https://orcid.org/0000-0003-1756-0162)

Atsushi Matsuoka[2,3] (matsuoka@geo.niigata-u.ac.jp)

Katsunori Kimoto[4] (kimoto@jamstec.go.jp)

Naoko Kishimoto[5] (kishimoto@kwansei.ac.jp)

[1] Department of Mechanical Engineering, Toyo University, Kujirai 2100, Kawagoe 350-8585, Japan

[2] Department of Geology, Niigata University, 8050, Ikarashi 2-no-cho, Nishi-ku, Niigata 950-2181, Japan

[3] Ocean Resources Research Center for Next Generation, Chiba Institute of Technology, 2-17-1 Tsudanuma, Narashino-shi, Chiba 275-0016, Japan

[4] Research Institute for Global Change, Japanese Agency for Marine-Earth Science and Technology, Natsuhimacho 2-15, Yokosuka 237-0061, Japan

[5] Faculty of Engineering, Kwansei Gakuin University, Gakuen Uegahara 1, Sanda 669-1330, Japan

Geometrical Variations of the Skeletal Structures of Genus *Pantanellium* as Determined from Collected Specimens

Takashi Yoshino*[1], Atsushi Matsuoka[2,3], Katsunori Kimoto[4], and Naoko Kishimoto[5]

[1]Department of Mechanical Engineering, Toyo University, Kujirai 2100, Kawagoe 350-8585, Japan

[2]Department of Geology, Niigata University, 8050, Ikarashi 2-no-cho, Nishi-ku, Niigata 950-2181, Japan

[3]Ocean Resources Research Center for Next Generation, Chiba Institute of Technology, 2-17-1 Tsudanuma, Narashino-shi, Chiba 275-0016, Japan

[4]Research Institute for Global Change, Japanese Agency for Marine-Earth Science and Technology, Natsuhimacho 2-15, Yokosuka 237-0061, Japan

[5]Faculty of Engineering, Kwansei Gakuin University, Gakuen Uegahara 1, Sanda 669-1330, Japan

Abstract

*Correspondence: tyoshino@toyo.jp. ORCID: https://orcid.org/0000-0003-1756-0162

Novel graph and string representations of the cortical shell structures of the genus *Pantanellium*, a Mesozoic radiolarian, are proposed. The representations are then used to compare the frame structures of fifty-nine specimens collected for the study. Among the fifty-nine fossil specimens, forty-seven different structures were found. It was also found that the frequency of the truncated icosahedron structure deviates significantly from the others. Although the proposed representations work well as a means of approximating and comparing frame structures, they appear to be too sensitive to classify the specimens.

Keywords: *Pantanellium*, skeletal structures, polyhedron geometry, planar graph

1 Introduction

Three-dimensional (3D) data acquisition techniques for marine plankton have progressed significantly in recent years (Siccha et al., 2023; Ishida et al., 2015; Kachovich et al., 2019). These techniques enable us to closely observe the skeletal structures of specimens from various angles and to better understand their structures, allowing us to analyze them geometrically.

Genus *Pantanellium* is one of the representative Mesozoic radiolarians (Pessagno, 1977; Pessagno and Blome, 1980). It is well known that the skeletal structure of the genus is geometrically simple; its cortical shell can be approximated by a polyhedron with three-degree vertices, pentagons, and hexagons (e.g., Matsuoka et al., 2012). For this reason, the authors have discussed in previous works geometrical treatments of its skeletal structures: planar graphs, pore counting (Yoshino et al., 2014), and origami representations (Yoshino et al., 2020). Matsuoka et al. (2012) and Yoshino et al. (2015) introduced a planar graph representation of the skeletal structures of the shells. However, to date, no effective drawing methods to compare the skeletal structures have been proposed. In this research, we introduce two new representations that enable us to make such comparisons.

The automatic naming of convex polyhedrons has been discussed in fullerene chemistry. Manolopoulos et al. (1991) proposed a method to name the molecular structures of fullerenes

using planar graphs of their molecular structures. Although Manolopoulos et al. (1993) reported that some fullerene structures consisting of more than 400 atoms could not be named using the method, the application of the technique to the approximated polyhedral structures of *Pantanellium* is attractive since they have a polyhedral nature similar to that of fullerenes.

The research described in this paper was conducted using 3D data newly obtained from a micro X-ray CT. We set two objectives for the study: to develop representations to describe the skeletal structures of the specimens that were collected and to use these representations to compare the skeletal structures. The remainder of the paper consists of (1) descriptions of our approximation of the newly available 3D data using polyhedral frames and the procedure used to obtain the proposed representations (Sec. 2); (2) results of our geometrical comparisons of the skeletal structures (Sec. 3); and (3) a discussion of the representatives and the comparisons that were made, along with the limitations and challenges of our work (Sec. 4).

2 Method

In this section, we outline the process of converting the 3D data of our specimens to two representations: a graph or two-dimensional (2D) representation, and a sequential or one-dimensional (1D) representation. Because approximately twenty specimens were scanned simultaneously for each measurement, we first describe separating the gross data into 3D data for each specimen. We next summarize the methods for approximating the skeletal structures of the frame structures introduced in our previous paper. Finally, we describe the procedure for obtaining the 1D and 2D representations. We implemented all the numerical processes using Mathematica® except for graph drawings.

2.1 Specimen description and 3D data acquisition

The radiolarian specimens were sampled from a sedimentation rock collected at the outer slope of the Mariana Trench. They differ from those used in our previous papers (e.g., Matsuoka et al., 2012), although their source is the same. In other words, we collected new specimens from the rock sample. *Pantanellium* species commonly have a porous spherical or subspherical cortical (outer) shell with bipolar primary spines and a spherical medullary (inner) shell. As shown in Fig. 1, we adopted the terminology proposed by Pessagno (1977) for the skeletal structures of the genus *Pantanellium*. The main features are the cortical shell and the primary spines. The former can be regarded as a massive frame of a spherical polyhedron (a polyhedron whose vertices consist of points on a sphere); the latter can be considered as the spines directed oppositely on the same line through the center of the cortical shell. Most pore frames (polygonal pores) are pentagonal or hexagonal, and most vertices are of degree three, that is, vertices consisting of three edges. We seldom observe quadrilateral or heptagonal pore frames or vertices of degree four. The primary spines and the cortical shell are connected so smoothly that the sections of the primary spines are Y-shaped, reflecting the arrangement of the pore frames. The Y-shape section results in the parts of the spines being termed ridges and grooves (Fig. 1).

We obtained our 3D data using the micro-X-ray CT system at JAMSTEC (see Kimoto et al., 2023). The large stage of the micro X-ray CT system enabled us to obtain the 3D structures of approximately twenty specimens simultaneously for each measurement. We took three measurements and obtained 3D data for fifty-nine specimens. The images in Fig. 2 show the projections of the raw 3D data onto a 2D plane.

2.2 Outline of data processing

We focused our attention on the frame structures of the cortical shells and the locations of the connections between the primary spines and the cortical shells. We approximated the cortical shell structures with the frames of spherical polyhedrons and represented the locations of

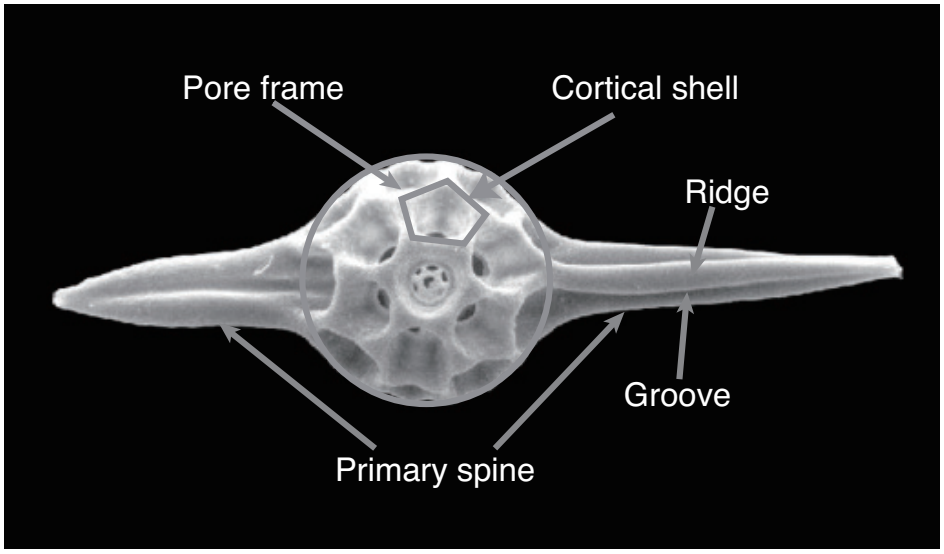

Figure 1: Terminology of *Pantanellium*.

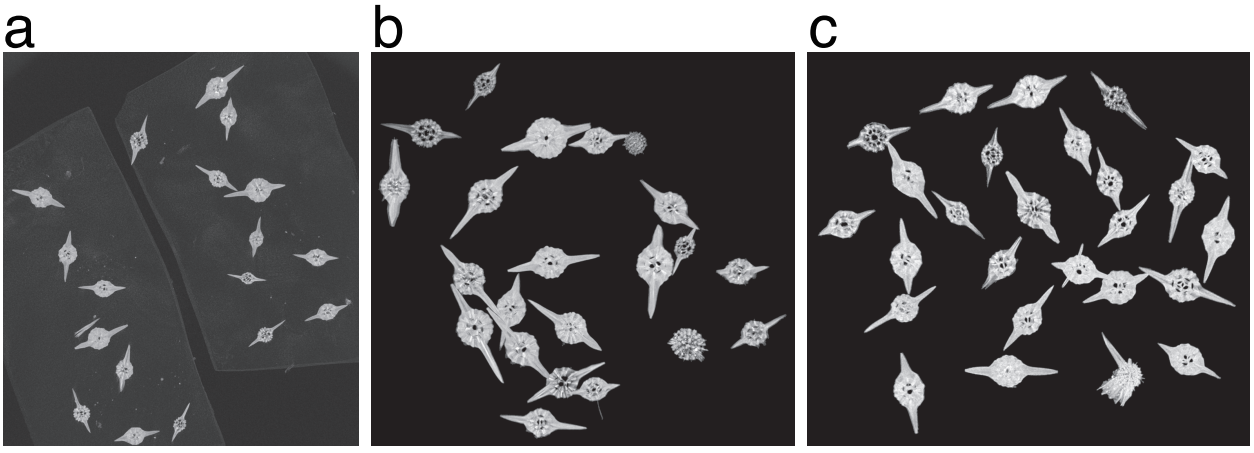

Figure 2: Two-dimensional projections of the original 3D images.

the primary spines using two vertices of the approximated polyhedrons corresponding to the connected parts. Figure 3 illustrates the approximation using one of the 3D observations as an example. The original data in Fig. 3a is approximated by a frame structure with the two unique vertices denoted as small spheres (Fig. 3c). Using semi-transparency, Fig. 3b shows the correspondence between the original data and the approximated structure. We ignored the inside part having a similar structure to the cortical shell since, in many cases, it had been lost during fossilization. Thus, the approximated data of a specimen include the frame structure of the approximated polygons and the two vertices corresponding to the locations of the primary spines.

The process of converting the obtained 3D data to planar graphs (2D representations) consists of two steps: preprocessing and graph drawing. The first step (preprocessing) approximates the 3D data using the frames of spherical polyhedrons; the second (graph drawing) transforms the frame structures into planar graphs. As a result, the 3D data of each specimen are converted into a combination of 1) the positions of the vertices, 2) pairs of vertex numbers describing the edges of the polyhedrons, and 3) two vertex numbers representing the locations of the primary spines. Note that the planar graph represents not the shapes of the polygons but rather their arrangement.

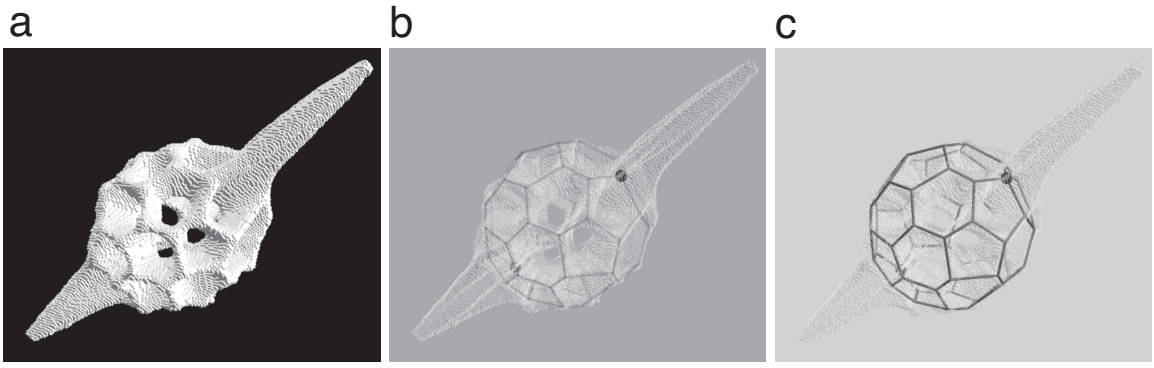

Figure 3: Comparison of the original 3D data and the approximated frame.

2.3 Preprocessing

Preprocessing involves the separation of individual specimens in raw data files using the following two steps: first, all the voxels of the 3D data are binarized into either zero or one based on a suitable threshold value. Next, the 3D data are divided into connected clusters, as shown in Fig. 4a. The *MorphologicalComponents* function of Mathematica was generally used for the separation; however, it was necessary to separate some of the connected specimens manually in cases where the divided data contained two connected specimens (Fig. 4b).

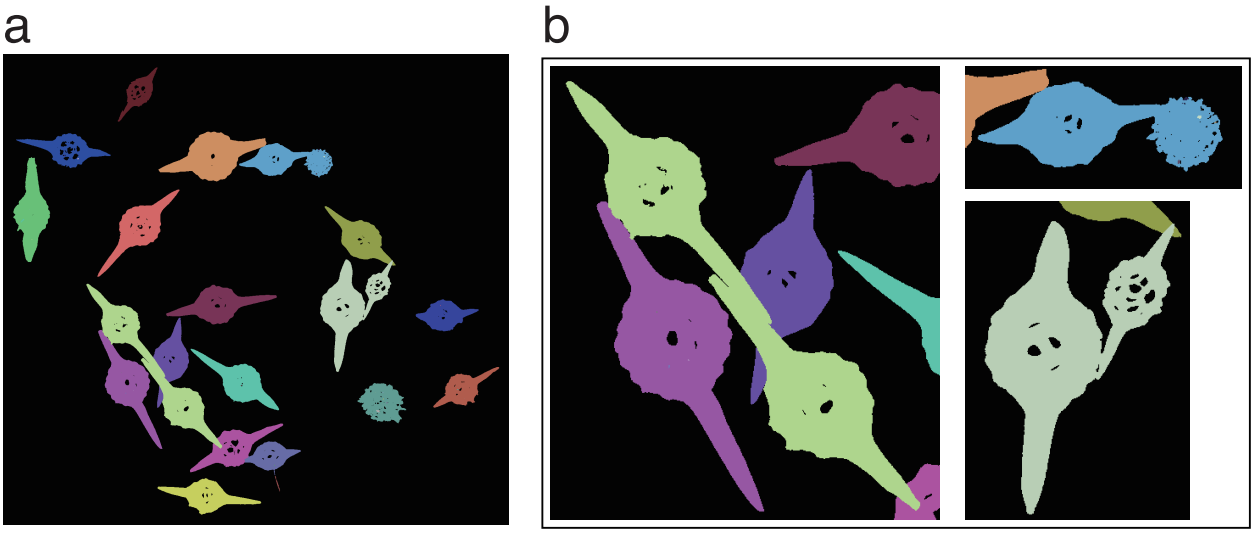

Figure 4: An example of the automatic separation (a: whole image, b: selected areas representing the connected cases in the entire image).

The second step of the preprocessing approximates the cortical shell structures to the frames of spherical polyhedrons. Here, we obtained the frame structures using the method proposed by Yoshino et al. (2014). The procedure assumes that the cortical shell structures can be regarded as Voronoi polyhedrons constructed based on the centroids of pores. The following is a summary of the procedure: 1) voxels not belonging to the cortical shells (e.g., the voxels that are parts of primary spines or inner shells) are removed by setting the range of the distance from the centroid of the data, 2) the centroids of the remaining voxels are projected onto the surface of a unit sphere whose center is located on the centroid of the remaining voxels, 3) the projected spherical points are approximated to the vertices of a

geodesic grid (a triangular grid on a sphere), 4) a low pass filter is applied to the data, 5) the individual pores are determined and the centroids of the pores are calculated, 6) a spherical Voronoi tessellation is produced based on the distribution of the centroids of the pores, and 7) the locations of the primary spines are determined by choosing the vertices closest to the primary spines.

2.4 Drawing rules of planar graphs

We created planar graphs to represent the 3D frame structures two-dimensionally. Since the graph must show the same edge connections as the polyhedral frames, the edge number of each pore frame is retained. The graphs are drawn based on the circular grid illustrated in Fig. 5a (whole structure) and 5b (closed view around the center). The basic rules for drawing the graphs are 1) the locations of the vertices are restricted only to the grid points, 2) edges connecting the vertices to represent the frames are not crossed, and 3) the shapes of all the polygons are convex. As shown in Fig. 5c, the frame structure of the specimen is drawn as a graph based on the grid. The white or transparent polygons represent the hexagonal pore frames, light gray is used for the pentagonal polygons, and dark gray is used for the others (quadrilateral or heptagonal). Drawing the graphs consists of three steps: 1) locating the two vertices representing primary spines, 2) determining the arrangement of the polygons around the center, and 3) allocating the other vertices and drawing all the edges. The following are detailed descriptions of the first and second steps.

One of the two vertices representing the primary spines is chosen and located at the center of the diagram, and another vertex is located at three different grid points on the outermost circle; these are either disks or circles in Fig. 5a. In other words, the opposite vertex is represented by three grid points: circles or disks. The representation of a vertex with three different grid points is a typical difference from the general planar graphs used in polyhedron geometry. Our observational data confirm that the two vertices corresponding to the location of the primary spines are of degree three (i.e., are Y-shaped). For this reason,

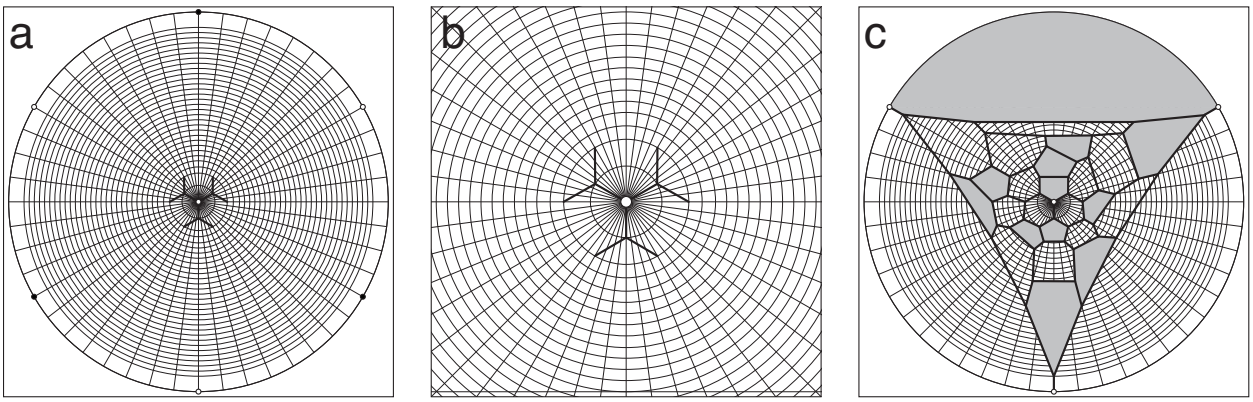

Figure 5: Template for drawing graphs and an example (a: whole view; b: closed view around the center; c: overlap of an example graph).

to fix the rules for drawing the graphs, we assume that the two vertices are always of degree three. The three outermost grid points reflect the geometrical relation between the primary spines. We classify the configuration of the two vertices into two types in order to select the disks or circles shown in Fig. 5a. One of two types of configurations—either "overlapped" (cis type) or "twisted" (trans type)—is chosen by observing the frame structure. Figure 6 shows the procedure: a frame is set so that one of the vertices is front and the other is back (Fig. 6a). The configuration of the overlap is then approximated as one of the two types (Fig. 6b). Circles are chosen in Fig. 5a if the relation is cis type; otherwise, disks are selected.

The three polygons around the center are drawn based on the pre-existing thick lines shown in Fig. 5b. We set the arrangement of the three polygons at the center to be mirror-symmetrical with a vertical line through the center, as shown in Fig. 7. The observational data support the notion that the polygons around the two vertices are pentagons and/or hexagons. Therefore, the planar graphs around the center can be considered one of four types, classified by the number of pentagons (0 to 3) composing the vertex. Figure 7 shows, from left to right, the cases of three, two, one, and zero pentagons. Such a restriction is useful for considering the symmetry properties of individual frame structures. After setting the central part, the rest of the polygons are drawn by locating the remaining vertices following our graph drawing rules, as demonstrated in Fig. 5c. Since two vertices can be

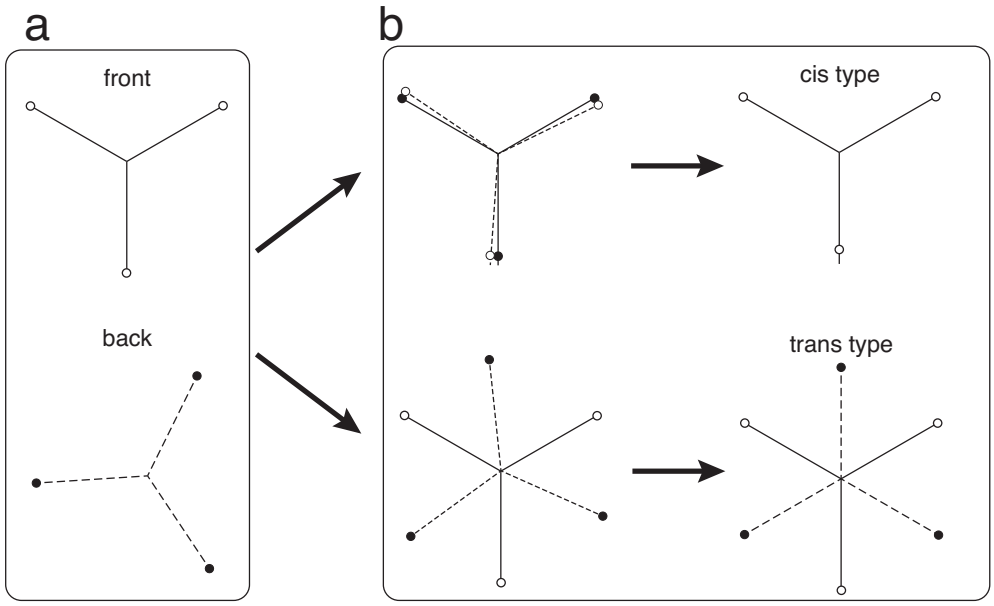

Figure 6: Two types of configurations of two primary spines.

chosen as the vertex at the center, two graph representations are produced for each specimen.

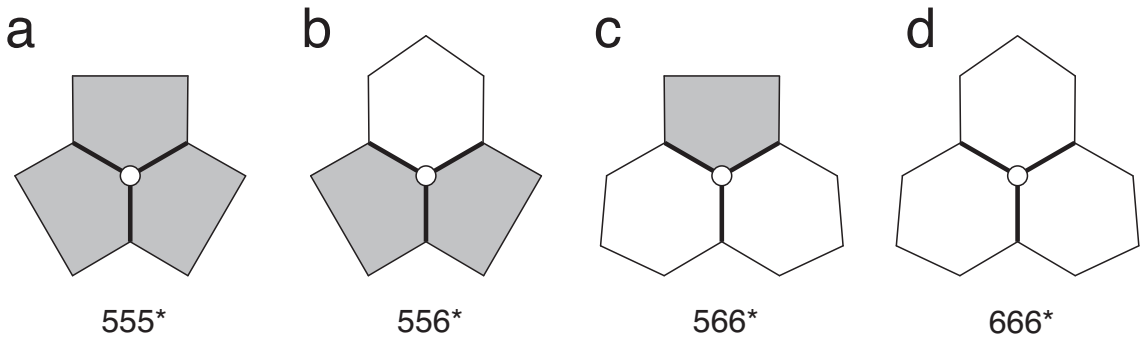

Figure 7: Four configurations around the vertex corresponding to a primary spine.

2.5 Sequential representations (one-dimensional representation)

Based on the 2D representations described above, we produced a 1D representation of the frame structures by modifying the method of Manolopoulos et al. (1991) using a sequence of digits (although, as mentioned in Manolopoulos and Fowler (1993), the method is not perfect). Such a 1D representation is worthy of consideration as it enables us to easily compare structures using a computer.

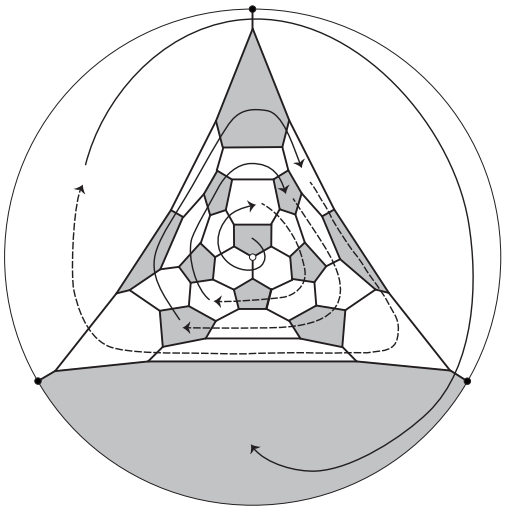

56666 65656 56565 66565 65656 56666 65t

Figure 8: 1D and 2D representations of a specimen having a truncated icosahedral structure.

The 1D representation consists of a sequence of digits representing the shapes of the pore frames (number of polygon edges), with a character added at the end. The digits are determined based on an imaginary spiral drawn clockwise from the center outward. Figure 8 shows an example of the spiral and the resulting sequence for a truncated icosahedral frame. For easier reading, the sequence has a space separating each grouping of five digits. Since there are three polygons at the center, there are three candidates for the beginning of the sequence.

To determine the 1D representation, one of the three possible representations is selected using the following rule. The digits are regarded as numbers, the smallest of which is chosen as the representative. Since the number of digits (number of pore frames) is the same for all the candidates, the early appearance of five (or four) is the key to identifying the spirals. As an example, the graphs in Fig. 7 are shown with their corresponding first three digits. The beginnings of the spiral are chosen as the pentagon at the right bottom (Fig. 7b) and the pentagon at the top (Fig. 7c). The arrangement around the three polygons at the center determines the beginning in other cases (Figs. 7a and 7d). The rule is also applied to the two graphs obtained from the two primary spines of a specimen. Finally, the representative

is determined. The letter 'c' or 't' is then added to the last digit to designate the relation between the primary spines: 'c' for cis and 't' for trans. To illustrate, the graph of the truncated icosahedral frame shown in Fig. 8 is described by the thirty-two-digit, one-letter sequence 56666 65656 56565 66565 65656 56666 65t.

3 Results

As described in Fig. 1, fifty-nine collected specimens were determined to be members of the genus *Pantanellium*. Using these specimens, we compared the 1D and 2D representations for each number of pore frames. Data obtained from our previous research were omitted. The frequencies of the various pore frame numbers and the results for specimens having thirty-two pore frames and those having twenty-seven pore frames, along with their 1D representations, are detailed below.

3.1 Whole view and thirty-two pore frames

Figure 9 shows the frequency distribution of the pore frame numbers and the approximated distribution curve. The mean and sample variance of the observed data were 27.4 and 10.4, respectively. Because the frequency of the specimens with thirty-two pore frames did not match the trend of the frequency distribution, we omitted these specimens from our estimation of the approximated curve (the dotted curve in Fig. 9). The mean and variance of the remaining forty-nine specimens were 25.4 and 6.8, respectively. Because of the asymmetric nature of the distribution, we assumed that the occurrence followed the log-normal distribution

$$p(x) = \frac{1}{\sqrt{2\pi}\,\sigma x} \exp\left(-\frac{(\log x - \mu)^2}{2\sigma^2}\right). \tag{1}$$

The estimated values of the distribution's two parameters were $\mu = 3.27$ and $\sigma = 0.0946$. The estimated curve in Fig. 9 thus becomes $y(x) = 49p(x)$ automatically since we estimated

the curve using forty-nine specimens. The expected values of the mean and variance from the distribution were $\mathrm{E}(X) = 26.4$ and $\mathrm{V}(X) = 6.27$, respectively.

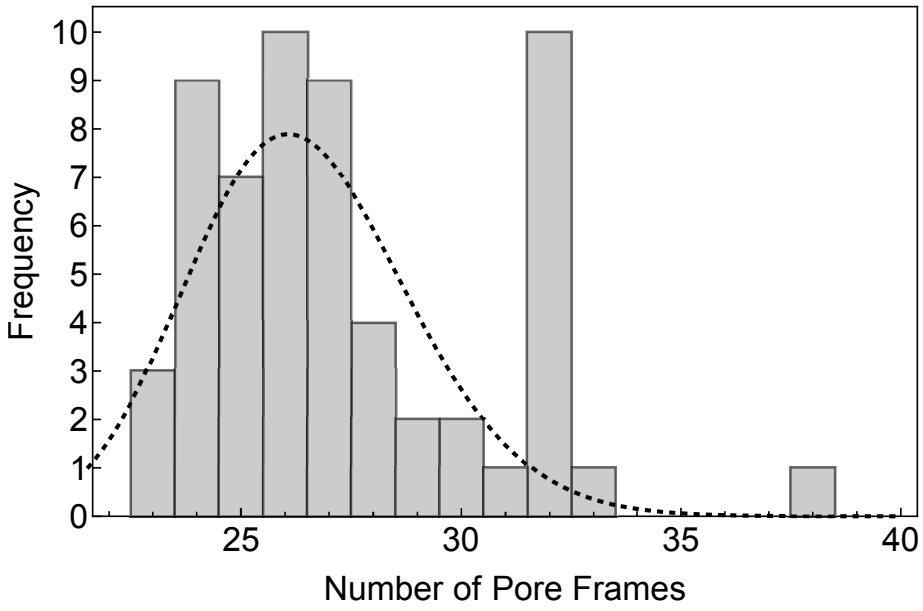

Figure 9: Frequency distribution and the estimated curve for the number of pore frames.

Although we omitted the thirty-two pore specimens from our estimation of the frequency distribution curve, its structure is representative from the viewpoint of both statistics and geometry. All ten specimens have the same structure as a truncated icosahedral frame. The 1D and 2D representations were shown earlier in Fig. 8.

The 1D representations of all fifty-nine specimens are listed in the Appendix. It should be noted that we failed to obtain a 1D representation for one of the two graphs of a specimen with twenty-three pore frames. The spiral was terminated when all the neighboring polygons of the one selected had already been chosen. In this case, we set the result of the 1D representation to "not available" and used another 1D and 2D representation obtained from a different central vertex. The number of 5s in the sequences is mostly twelve since most frames consist of pentagons and hexagons and degree-three vertices (Matsuoka et al., 2012; Yoshino et al., 2015). Other numbers of pentagons indicate that the frame has a quadrilateral, heptagon, or a vertex of degree four, as noted later.

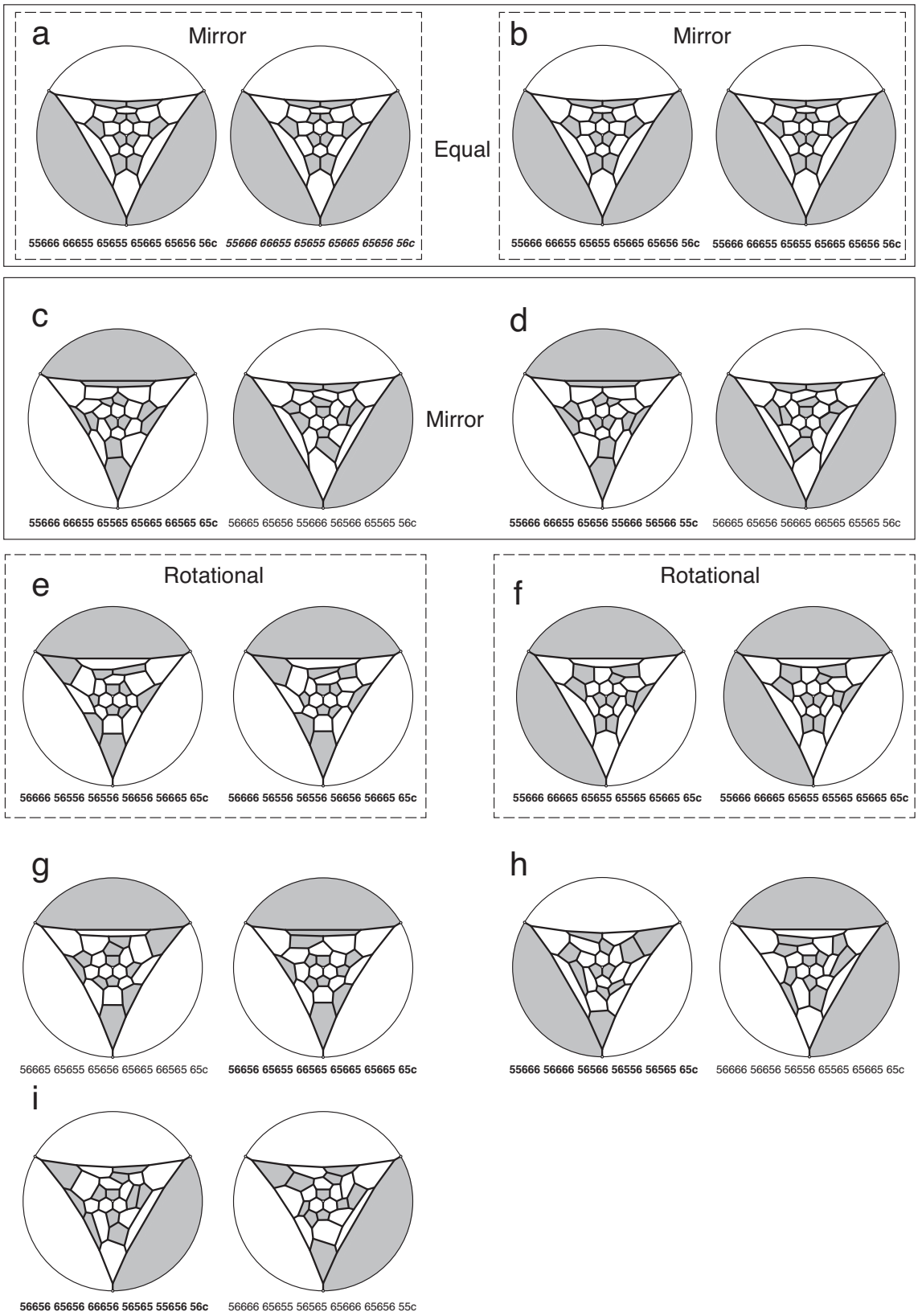

Figure 10: All planar graphs of twenty-seven pore frame specimens.

3.2 Specimens having twenty-seven pore frames

As an example of our results, we show in Fig. 10 the planar graphs and the 1D representations of all the specimens with twenty-seven pore frames (nine specimens) using the proposed method. Two 1D and 2D representations are shown for each specimen using a different vertex at the center. The selected 1D representation appears in bold type. Only one geometrically equal pair was found (Figs. 10a and 10b), meaning that there were eight geometrically different structures among the nine specimens. We also found a pair with a mirror symmetry relation (Figs. 10c and 10d), where the original frame and its mirror image are located side by side. Because this had not been discovered from their 1D representations, we regarded them as different structures. In addition, it makes clear that the last three digits of the 1D representation do not always represent the arrangement around the opposite primary spine.

Some specimens had symmetrical features—rotational symmetry (Figs. 10e and 10f) and mirror symmetry (Figs. 10a and 10b)—in their structures. With the former, the two sequential representations of the specimen are the same. On the other hand, the latter is not found from a comparison of 1D representations but from a comparison of the two graph representations. As mentioned, the graph representation was designed to find mirror symmetry with a vertical line (plane in 3D) through the center. The equivalence between a 1D representation and the reverse order of another 1D representation is not necessary but sufficient for mirror symmetry. In other words, the mirror symmetry feature is possible even if the two 1D representations are different, as shown in Figs. 10a and 10b. It should be noted that mirror symmetry automatically satisfies the condition of rotational symmetry.

3.3 Comparisons of the one-dimensional representations

The same structures were searched by comparing the 1D representations of specimens with the same pore frame numbers. Such structures were found for twenty-four pore frames, twenty-seven pore frames (Figs. 10a and 10b), and thirty-two pore frames (Fig. 8b). For the twenty-four pore frames, three specimens had the same 1D representation: 55666 66565

65655 56556 5566c. As a result, we found forty-seven different structures among our fifty-nine specimens.

Specimens with the same digits but a different last character were observed for the cases of twenty-four and twenty-six pores. Figure 11 shows the case of twenty-four pore frames. We regarded the specimens as different because the graphs and sequences were different. However, the frame structures of the cortical shells were the same. The locations of the primary spines are responsible for the difference. The location of the primary spine on the back of the specimen in Fig. 11a was the right bottom vertex consisting of two pentagons and a hexagon, indicated by the arrow in Fig. 11b.

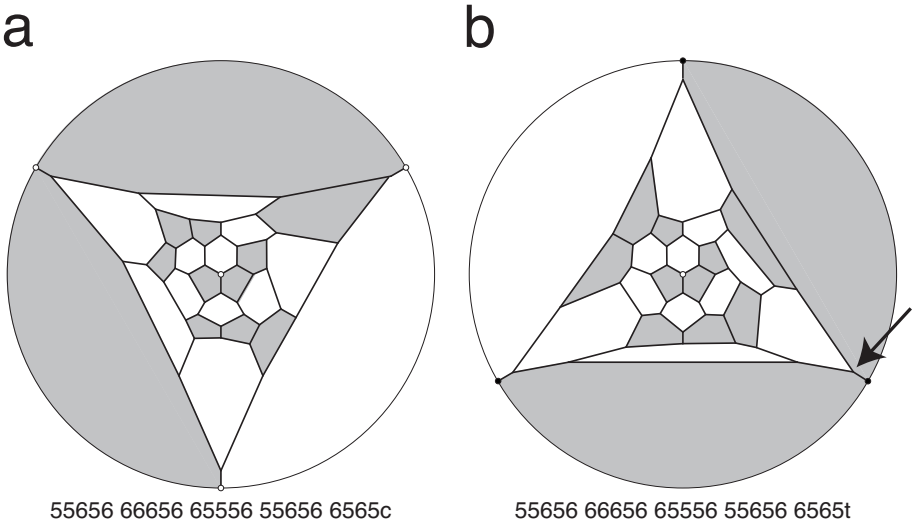

Figure 11: Two graphs showing different locations of primary spines.

Most 1D representations contained twelve 5s (pentagonal frames), as noted above; however, some specimens involved a different number of 5s. The specimen with only ten 5s included a '4' (quadrilateral), while the one with thirteen 5s included a '7' (heptagon). The results were geometrically correct since they satisfied the following equation derived from Euler's polyhedron formula (Coxeter, 1989), under the condition that all the vertices are of either degree three or four:

$$\sum_{n=3}^{\infty}(6-n)f_n - 2v_4 = 12, \tag{2}$$

where f_n and v_4 denote the number of n-gons and the number of vertices of degree four, respectively. It is apparent from the equation that the number of hexagons does not affect the number of other polygons. Similarly, fourteen 5s were observed twice for the specimens consisting of pentagonal and hexagonal pore frames, and both specimens contained a vertex of degree four. They also satisfied the above equation.

4 Discussion

We proposed 1D and 2D representations describing the cortical shell structures of the genus *Pantanellium*. These representations enabled us to compare the structures of our collected set of specimens. Our method revealed that cortical shells vary with respect to the number of pore frames and geometrical structure. Although we believe that our proposed method provides an effective way to describe and compare frame structures for the genus *Pantanellium*, it appears to be too sensitive to support a new classification as the results indicated that most specimens differed from one another.

The proposed method presents new issues since such a geometrical treatment has not previously been attempted. For example, should we regard the two specimens with mirror-symmetrical opposite structures as different? In chemistry, they are treated differently in terms of "geometrical isomers." However, in our case, the function is biologically equivalent. We regarded them as different in this paper since they could not be detected by comparing 1D representations; however, this reason is not particularly strong.

The geometric feature of the frame structures commonly observed among the specimens remains unclear. We discussed the distribution of pentagons in our previous works; however, as yet, no standard features have been found. The deviation of the frequency of thirty-two pore specimens from the frequency distribution might be one of the keys to finding these features since the frame structure consists of isolated pentagons, and all pentagons are surrounded by hexagons.

Importantly, our method can be executed automatically, although all the 1D and 2D representations were obtained manually in this research. The projection from a 3D frame to a graph on the grid and the selection of polygons spirally should be easy to incorporate into a computer program. On the other hand, selecting the two vertices corresponding to the locations of the primary spines will be somewhat more complicated since the program must have a routine for determining the voxels comprising the primary spines. However, automating the generation of our proposed representations should produce more statistically accurate results as it will enable us to produce geometrical data for a very large number of specimens.

Declaration of Interest

The authors declare no competing interests.

Acknowledgments

This research was supported by the Ministry of Education, Science, Sports and Culture (MEXT), Grant-in-Aid, No. 21K03376 (T.Y.) and No. 20K04144 (A.M.).

Author contributions. T.Y. performed the data analysis and wrote the manuscript. A.M. selected specimens and acquired 3D data. K.K. and N.K. acquired 3D data.

Data availability. The 1D string representations for all 59 specimens are provided in the Appendix. The 3D CT data are not publicly available due to the large file size. Other data supporting the findings of this study are available from the corresponding author upon reasonable request.

Declaration of generative AI and AI-assisted technologies in the writing process. During the preparation of this work, the authors used Claude (Anthropic) to improve the

language and adapt the manuscript to journal submission guidelines. After using this tool, the authors reviewed and edited the content as needed and take full responsibility for the content of the published article.

References

Coxeter, H.S.M., 1989. Introduction to Geometry, 2nd ed. Wiley.

Ishida, N., Kishimoto, N., Matsuoka, A., Kimoto, K., Kurihara, T., & Yoshino, T., 2015. Three-dimensional imaging of the Jurassic radiolarian *Protunuma?ochiensis* Matsuoka: an experimental study using high-resolution X-ray micro-computed tomography. *Volumina Jurassica*, 13(1), 77–82.

Kachovich, S., Sheng, J., & Aitchison, J.C., 2019. Adding a new dimension to investigations of early radiolarian evolution. *Scientific Reports*, 9(1), 6450.

Kimoto, K., Horiuchi, R., Sasaki, O., & Iwashita, T., 2023. Precise bulk density measurement of planktonic foraminiferal test by X-ray microcomputed tomography. *Frontiers in Earth Science*, 11, 1184671. `https://doi.org/10.3389/feart.2023.1184671`

Matsuoka, A., Yoshino, T., Kishimoto, N., Ishida, N., Kurihara, T., Kimoto, K., & Matsuura, S., 2012. Exact number of pore frames and their configuration in the Mesozoic radiolarian *Pantanellium*: an application of X-ray micro-CT and layered manufacturing technology to micropaleontology. *Marine Micropaleontology*, 88, 36–40. `https://doi.org/10.1016/j.marmicro.2012.02.005`

Manolopoulos, D.E., May, J.C., & Down, S.E., 1991. Theoretical studies of the fullerenes: C34 to C70. *Chemical Physics Letters*, 181(2–3), 105–111.

Manolopoulos, D.E., & Fowler, P.W., 1993. A fullerene without a spiral. *Chemical Physics Letters*, 204(1–2), 1–7.

Pessagno, E.A., Jr., 1977. Upper Jurassic radiolaria and radiolarian biostratigraphy of the California Coast Ranges. *Micropaleontology*, 23, 56–113.

Pessagno, E.A., Jr., & Blome, C.D., 1980. Upper Triassic and Jurassic Pantanelliinae from California, Oregon and British Columbia. *Micropaleontology*, 26, 225–273.

Siccha, M., Morard, R., Meilland, J., Iwasaki, S., Kucera, M., & Kimoto, K., 2023. Collection of X-ray micro computed tomography images of shells of planktic foraminifera with curated taxonomy. *Scientific Data*, 10(1), 679.

Yoshino, T., Kishimoto, N., Matsuoka, A., Ishida, N., Kurihara, T., & Kimoto, K., 2014. Pores in spherical radiolarian skeletons directly determined from three-dimensional data. *Forma*, 29, 21–27.

Yoshino, T., Matsuoka, A., Kurihara, T., Ishida, N., Kishimoto, N., Kimoto, K., & Matsuura, S., 2015. Polyhedron geometry of skeletons of Mesozoic radiolarian *Pantanellium*. *Revue de Micropaléontologie*, 58(1), 51–56. https://doi.org/10.1016/j.revmic.2015.01.002

Yoshino, T., Matsuoka, A., & Kishimoto, N., 2020. Origami reconstruction of the cortical shell structures of radiolarian genus *Pantanellium* from planar graphs. *Revue de Micropaléontologie*, 67, 100423.

A 1D representations of all 59 specimens

The numbers in parentheses indicate the number of specimens having the same structure.

23 pore frames

- 56656 65656 56555 65565 665 c
- 55665 66565 56655 65655 656t
- 56665 65655 55656 55666 565 c

24 pore frames

- 56656 65565 65655 66556 5656t
- 55656 66656 65556 55656 6565 c
- 55656 66656 65556 55656 6565t
- 55666 66565 65655 56556 5566 c (3)
- 55666 66655 55655 55666 5665t
- 56665 65655 56565 65665 6565 c
- 55656 66656 65556 56556 6556 c

25 pore frames

- 55656 65656 65665 66556 56565 c
- 55666 65565 55656 55566 65565t
- 55656 66656 66555 65655 56656 c
- 55666 66655 65655 56566 55665 c
- 55665 66656 56555 56556 55566t
- 55666 66655 56555 65665 66556 c
- 55666 66556 55656 56656 55656t

26 pore frames

- 55666 66656 55655 65565 65656 6 c
- 56656 66565 65655 56565 65665 6 c
- 56656 65655 66565 65665 56565 6 c
- 56656 65655 66565 65665 56565 6t
- 56656 56565 66565 65656 56656 5 c

- 55666 66655 65655 65665 56655 6 c
- 56665 66556 55665 65656 56556 6 c
- 56666 55656 56566 66556 55655 6 c
- 56656 65655 66655 65665 55665 6 c
- 56656 56565 66665 65656 46565 6 c

27 pore frames

- 55666 66665 65655 65565 65665 65 c
- 55666 66655 65655 65665 65656 56 c (2)
- 56656 65655 66565 65665 65665 65 c
- 55666 66655 65565 65665 66565 65 c
- 55666 66655 65656 55666 56566 55 c
- 56666 56556 56556 56656 56665 65 c
- 56656 65656 66656 56565 55656 56 c
- 55666 56666 56566 56556 56565 65 c

28 pore frames

- 55666 66656 65656 55655 65656 665t
- 56666 56656 55665 65565 66556 656t
- 56666 56556 56656 56656 55566 566 c
- 56656 65565 66656 66565 56565 665 c

29 pore frames

- 56665 65656 56666 55656 55566 6665 c
- 56665 65656 56656 65656 65665 6565 c

30 pore frames

- 55666 66665 65565 65566 56665 66565t
- 56665 66556 65665 56665 65666 56565 c

31 pore frames

- 55666 66665 65656 56556 56565 66666 5 c

32 pore frames

- 56666 65656 56565 66565 65656 56666 65t (10)

33 pore frames

- 56666 65566 57565 66656 56556 66565 656t

38 pore frames

- 56666 56665 65666 65656 66656 56656 56565 666 c